Wrinkling instability of 3D auxetic bilayers in tension*

Sairam Pamulaparthi Venkata[a,1], Yuxin Fu[b,1], Yibin Fu[c], Valentina Balbi[a] and Michel Destrade[a,d,*]

[a] School of Mathematical and Statistical Sciences, University of Galway, University Road, Galway, H91 TK33, Ireland
[b] Tainjin University, Hangzhou 310027, People's Republic of China
[b] Department of Mechanics, Tianjin University, Tianjin 300072, People's Republic of China
[c] School of Computer Science and Mathematics, Keele University, Staffs ST5 5BG, United Kingdom
[d] Key Laboratory of Soft Machines and Smart Devices of Zhejiang Province and Department of Engineering Mechanics, Zhejiang University, Hangzhou 310027, People's Republic of China

ARTICLE INFO

Keywords:
Auxetic materials
Hyperelasticity
Tension instability
Bilayer wrinkling
Controlled buckling

ABSTRACT

Bilayers (soft substrates coated with stiff films) are commonly found in nature with examples including skin tissue, vesicles, or organ membranes. They exhibit various types of instabilities when subjected to compression, depending on the contrast in material properties between the two components. We present wrinkling instabilities for 3D hyperelastic bilayer systems, including auxetics (materials with negative Poisson's ratio), under uni-axial *tension*. In tension, a soft bilayer can experience large lateral contraction, and we find that with an adequate contrast in the Poisson ratios, compressive stresses may develop and generate wrinkles aligned with the tensile direction. We rely on an analytic modelling of the phenomenon, and validate it with a user-defined Python script with periodic boundary conditions and constitutive relation implementation in advanced Finite Element simulations. Our findings reveal that wrinkles are observed when the Poisson ratio of the substrate is greater than that of the film. As the two Poisson ratios converge to a common value, the critical stretch of instability shoots up rapidly, and the wrinkling disappears. We also confirm these results by asymptotic analysis. This wrinkling analysis has significant potential in controlling surface patterns of auxetic skin grafts and hydrogel organ patches under mechanical loads. Moreover, the asymptotic expressions in this work can be used under finite strain for buckling-based metrology applications.

1. Introduction

Auxetics, materials with negative Poisson's ratio, expand in all directions under uni-axial tension. For 3D isotropic materials with auxetic behavior, the theoretical value of Poisson's ratio ranges between -1 and 0.5 [1]. Thanks to rapid advancement in additive and subtractive manufacturing techniques [2, 3], along with extensive research on negative Poisson ratio materials, auxetics have shown promising applications in various fields [4–9].

Compliant substrates coated with thin-layered stiff films (bilayers) are commonly found in nature; for example, skin tissue consists of a thin, stiff epidermal layer attached to a thick, soft dermis. When subject to mechanical loads, bilayer systems can exhibit surface patterns through wrinkles. This instability phenomenon has found a broad range of applications, in optical sensors [10], novel flexible electronics [11–13], tunable phase gratings [14], buckling-based metrology [15, 16], surface wetting [17], and for buckling-related applications in soft matter [18].

The formation of these surface patterns is controlled by different parameters, such as the contrast in material properties [19, 20], differential growth [21], film-to-substrate thickness ratio [22, 23], initial imperfections [24], substrate nonlinearity [25, 26], interfacial mechanics [27, 28], etc.

A survey of the literature shows that wrinkles appearing in tension are seldom studied beyond the linear-elastic framework [29], although they have been established experimentally under large strains [15, 30], see Fig. 1. In this work, we perform a linear buckling analysis of 3D hyperelastic thin stiff films on semi-infinite compliant substrates (including auxetics) in *tension* and large strains, in contrast to the numerous existing studies concerned with compression.

We first use the buckling analysis available in ABAQUS [31], which works up to a point, beyond which we have to rely on a semi-analytical approach with Mathematica [32]. We find that wrinkles may be generated in bilayers subjected to uni-axial tension. Main and original findings include (i) Deriving asymptotic expressions for critical stretch ratios and critical wavenumbers, valid in finite strains and useful for buckling-based metrology applications; (ii) Showing that the Poisson ratio of the substrate must be greater than that of the film for wrinkles to appear; (iii) Establishing that wrinkles disappear when the Poisson ratios of film and substrate converge to a common value, and that (iv) The wrinkling wavelength is high (low) when the Poisson ratios of film and substrate are close (far).

2. Results

2.1. 3D bilayer system in tension

We consider 3D bilayer systems with a thin stiff film perfectly bonded to a semi-infinite compliant substrate, see Fig. 1. Under a uniaxial tension applied along the

* This research project is funded by the XS-META ITN: Marie Skłodowska-Curie European Actions (Grant Agreement No. 956401).
* Corresponding author
S.PamulaparthiVenkata1@universityofgalway.ie (S.P. Venkata); Y.Fu7@universityofgalway.ie (Y. Fu); y.fu@keele.ac.uk (Y. Fu); vbalbi@universityofgalway.ie (V. Balbi); michel.destrade@universityofgalway.ie (M. Destrade)
ORCID(s): 0000-0002-2409-7332 (S.P. Venkata); 0000-0002-7538-9490 (V. Balbi); 0000-0002-6266-1221 (M. Destrade)
[1] These authors contributed equally to this work.

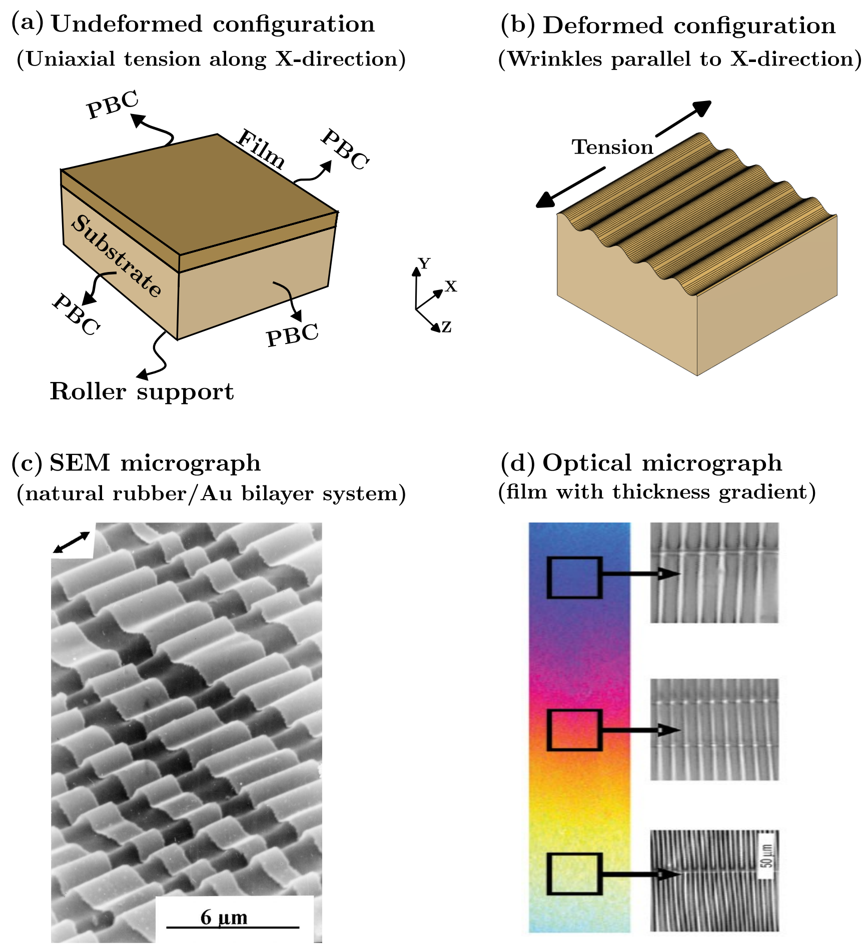

Figure 1: (a) Undeformed and (b) deformed configurations of a 3D bilayer system with periodic boundary conditions in the lateral directions. The system is infinite in the X- and Z-directions and is under uni-axial tension along the X-direction. The analysis shows that eventually, (b) wrinkles develop parallel to the X-direction, provided there is enough contrast between the constitutive parameters of the materials. (c) Image obtained using Scanning Electron Microscope (SEM) on a natural rubber substrate coated with a gold film, when elongated to 50% strain at room temperature [30]. An inset with an arrow shows the direction of elongation. Bright and dark bands represent the buckled gold film layer and the rubber showing through cracks in the stretched film, respectively. (d) Optical micrograph of a Polystyrene (PS) film layer on a silicon wafer with decreasing thickness from top to bottom is shown on the left panel. The corresponding wrinkles exhibit decreasing wavelengths on the right panel, when the PS films are attached to a Polydimethylsiloxane (PDMS) substrate and elongated to induced buckling [15].

X-direction, the bilayer is expected to eventually develop wrinkles aligned with that direction, as shown in Fig. 1(b), provided compressive stresses develop along the Y-direction because of a sufficient Poisson ratio contrast.

Here we use the Blatz-Ko strain energy function [34] for both materials:

$$W = c_1 \left(I_1 - 3 + \frac{1}{\beta}\left(I_3^{-\beta} - 1 \right) \right) + c_2 \left(\frac{I_2}{I_3} - 3 + \frac{1}{\beta}\left(I_3^{\beta} - 1 \right) \right), \quad (1)$$

where $c_1 = \alpha\frac{\mu}{2}$, $c_2 = (1-\alpha)\frac{\mu}{2}$, $\beta = \frac{\nu}{1-2\nu}$, $\mathbf{F}$ is the deformation gradient, and $I_1 = \mathrm{tr}(\mathbf{F}\mathbf{F}^T)$, $I_2 = I_3\mathrm{tr}[(\mathbf{F}\mathbf{F}^T)^{-1}]$, $I_3 = \det(\mathbf{F}\mathbf{F}^T)$ are three strain invariants. Also, the material constants are the non-dimensional parameter $0 < \alpha < 1$, the initial shear modulus $\mu > 0$, and the Poisson ratio $-1 < \nu \leq 1/2$. We use the letters f and s for film and substrate, respectively. For the simulations, $\alpha_f = \alpha_s = 0.4$ and $\mu_f/\mu_s = 30$ (similar observations to those detailed in this study can be made for other values).

Auxetic materials are highly compressible due to their negative Poisson ratio (thus far away from the incompressibility limit of a Poisson ratio equal to 1/2). Blatz-Ko strain energy functions with a negative Poisson ratio can thus be used to model auxetics, although with certain limitations [35]. For example, Ciambella and Saccomandi [36] use the Blatz-Ko strain energy to capture the experiments of Choi and Lakes [37] on auxetic materials. The model is also adequate to capture the experimental behaviors of membranes (no substrate) under tension, from auxetic to conventional Poisson ratios, see Fig. 2.

Now, using the Blatz-Ko model for 3D bilayer systems under large uni-axial elongation, we find that wrinkles are

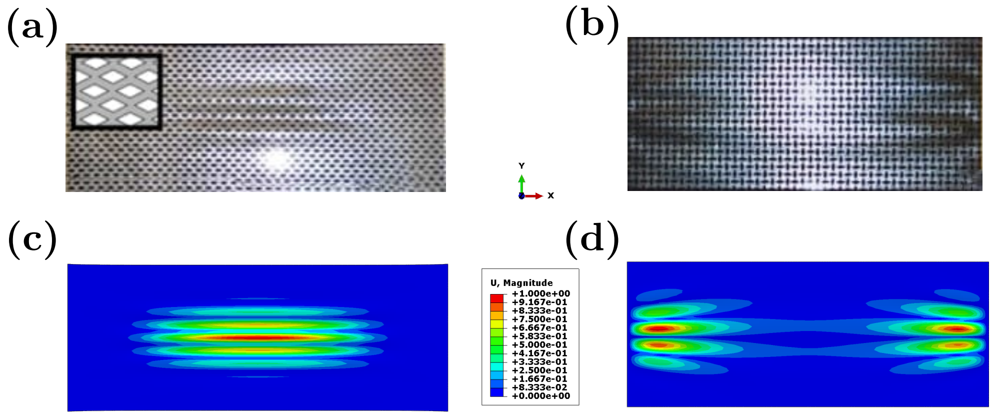

Figure 2: Comparison of wrinkling profiles in thin conventional and auxetic sheets. Top row: Thin acetate sheets under uni-axial tension, with (a) non-auxetic micro-structural patterns and (b) auxetic micro-structural patterns [33]. For conventional sheets, wrinkles develop at the center of the sheet. For auxetic sheets, they appear near the clamped edges. Bottom row: Buckling profiles (according to the magnitude of the displacement field) obtained with ABAQUS and the Blatz-Ko model Eq. (1). Here $\alpha = 0.4$, $\mu = 0.53$ GPa, and $\nu = 0.38, -0.2$ in (c) and (d), respectively.

observed only when the Poisson ratio of the film (ν_f) is smaller than that of the substrate (ν_s), as summarised in Fig. 3. This result recovers the work by Nikravesh et al. [38] conducted for linear-elastic bilayer systems.

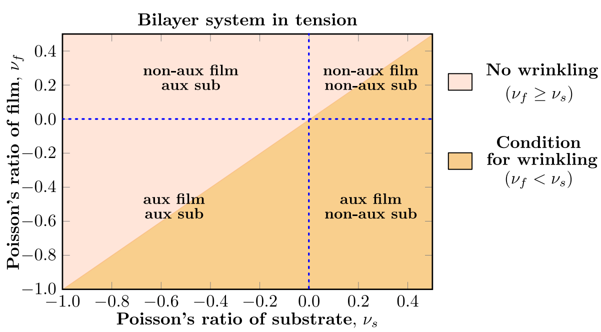

Figure 3: Wrinkling condition according to the contrast between the Poisson ratios of film and substrate.

2.2. Incompressible substrate

First, we assume that the substrate is quasi-incompressible ($\nu_s = 0.495$) while for the film, $\nu_f \in (-0.95, 0.495)$.

Here the Poisson ratio of the substrate is greater than that of film, and under uniaxial tension, the film expands more than the substrate along the Z-direction, resulting in compressive stresses and the formation of wrinkles parallel to the X-direction.

In Fig. 4(a-b), the values of the critical stretch of wrinkling λ_c and of the corresponding critical wavenumber k_c are plotted against ν_f. From Fig. 4a, we observe that the critical stretch ratio values predicted from the semi-analytical analysis (Mathematica) and the FE buckling analysis ABAQUS match well, as long as $\nu_f \leq 0.35$. Beyond this value, ABAQUS ceases to predict wrinkles in the desired direction and gives negative eigenvalues, suggesting the load direction has to be reversed to obtain wrinkles, which is unphysical.

An auxetic film ($\nu_f < 0$) expands in all directions under tension while the incompressible substrate contracts along the Z direction, leading to compressive stress in the film. Hence only low values of the critical stretch are required for the wrinkles to occur. As the Poisson ratio of the film increases and moves closer to that of the substrate, the values of the critical stretch shoot up sharply, supporting our findings in Fig. 3.

2.3. Highly auxetic film

Now we take the film to be highly auxetic, with Poisson ratio $\nu_f = -0.95$, while for the substrate, $\nu_s \in (-0.95, 0.495]$.

Fig. 4(c-d) show the variations of λ_c and k_c with ν_s. Again, we find good agreement between analysis and simulations for a certain range, when $-0.7 \leq \nu_s \leq 0.495$. For $\nu_s < -0.8$, ABAQUS stops providing meaningful predictions. In general, the buckling occurs early, except as $\nu_s \to \nu_f$ when it increases dramatically because in that limit, both film and substrate experience the same transverse contraction so that no compressive stress nor wrinkles develop. Similarly to Fig. 4b, Fig. 4d shows that the higher the Poisson ratio contrast is, the larger the wavelength of the wrinkles is.

In summary, we found that to ensure early wrinkling in tension, a large contrast in Poisson's ratio is required, for example by taking one material to be auxetic and the other non-auxetic.

2.4. Asymptotic solution: Compressible neo–Hookean bilayer system

The following critical strain and wavenumber expressions:

$$\epsilon_c = \frac{1}{4(\nu_s - \nu_f)} \left(3 \frac{\mu_s}{\mu_f} \frac{1-\nu_f}{1-\nu_s} \right)^{2/3},$$

$$k_c h = \left(3 \frac{\mu_s}{\mu_f} \frac{1-\nu_f}{1-\nu_s} \right)^{1/3}, \tag{2}$$

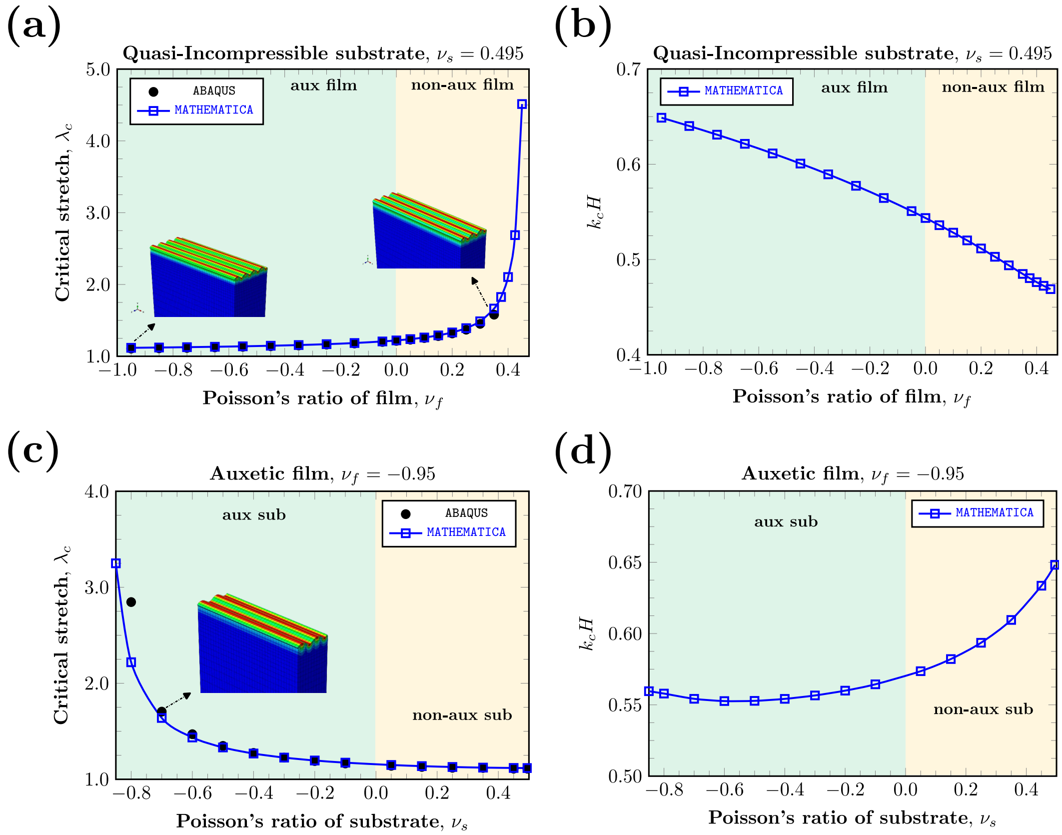

Figure 4: Numerical simulations using Blatz-Ko material model (Eq. (1)). Variations of the critical stretch of wrinkling λ_c and corresponding critical wavenumber measure $k_c H$ with the Poisson ratio of one layer (k_c is the critical wavenumber and H is the film initial thickness). (a-b): The substrate is quasi-incompressible ($\nu_s = 0.495$). (c-d): The film is highly auxetic ($\nu_f = -0.95$). Results from ABAQUS: black dots, results from Mathematica: solid line with square markers.

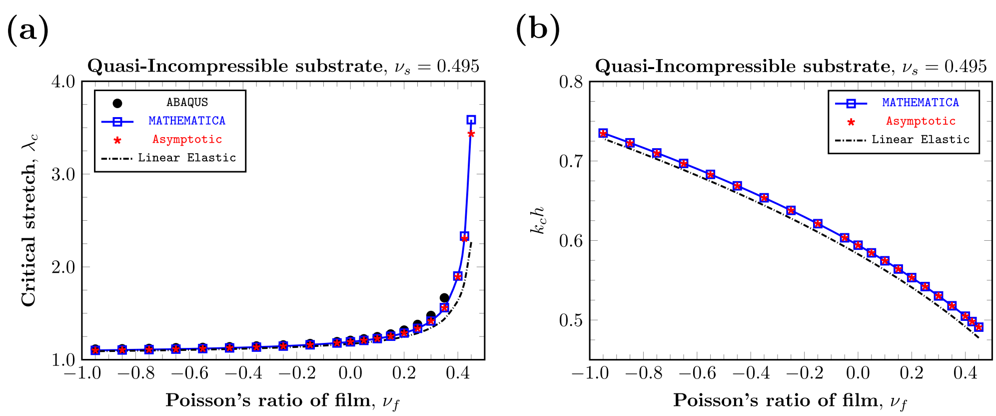

Figure 5: Numerical simulations for a bilayer made of compressible neo-Hookean materials ($\alpha_s = \alpha_f = 1$ in Eq. (1)). The substrate is quasi-incompressible ($\nu_s = 0.495$). (a-b): Variations of the critical stretch of wrinkling λ_c and corresponding critical wavenumber measure $k_c h$ (k_c: critical wavenumber, h: current film thickness) with the Poisson ratio of film layer ν_f. ABAQUS: black dots, Mathematica: solid line with square markers, Asymptotic expressions (Eqs. (3) to (4)): star markers, Linear-elastic expressions (Eq. (2)): dash-dotted line.

have been derived by [30, 38, 39] for linearly elastic bilayers under uniaxial tension. These expressions are valid under the plane-strain approximation. Here, h is the current thickness of the film, ϵ_c is the critical strain, and k_c is the critical wavenumber.

However, we note that the plane-strain assumption is not valid for a bilayer system under uni-axial tension. Here, we follow Cai and Fu [40, 41] and assume that the shear modulus ratio $r = \mu_s/\mu_f$ is of order $(k_c h)^3$ to derive asymptotic expansions for the critical strain and wavenumber (for

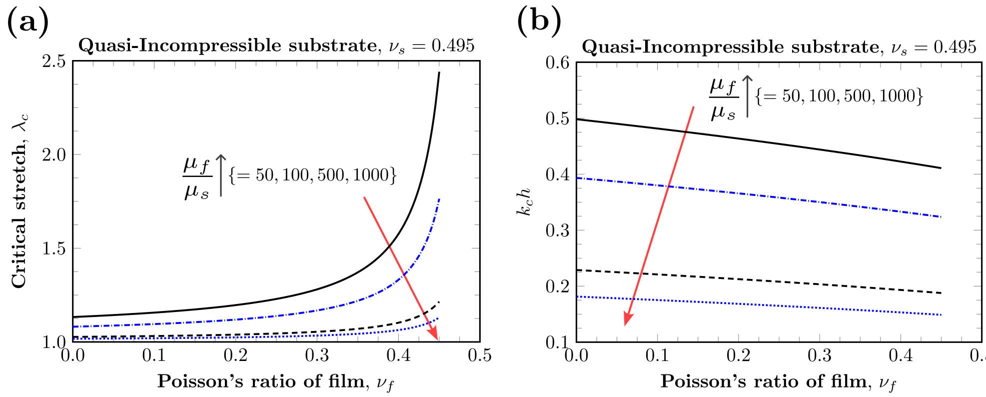

Figure 6: Using the asymptotic expressions Eq. (3)-Eq. (4) for compressible neo-Hookean materials ($\alpha_s = \alpha_f = 1$ in Eq. (1)). The substrate is quasi-incompressible ($\nu_s = 0.495$). (a-b): Variations of the critical stretch of wrinkling λ_c and corresponding critical wavenumber measure $k_c h$ with the Poisson ratio of film layer (k_c is the critical wavenumber and h is the deformed film thickness) and for contrast in shear moduli between the layers ($\mu_f/\mu_s = \{50, 100, 500, 1000\}$).

simplicity, we take $\alpha_s = \alpha_f = 1$ in Eq. (1)). We find

$$\lambda_c = 1 + \frac{\left[(1-\nu_f)(1-\nu_s)\right]^{2/3}}{(\nu_s-\nu_f)\left(8\nu_s/3-2\right)^{2/3}} r^{2/3} + \frac{(1-\nu_f)(2\nu_s-1)}{(\nu_s-\nu_f)(4\nu_s-3)} r + c_4 r^{4/3} + c_5 r^{5/3} + c_6 r^2 + \mathcal{O}(r^{7/3}), \tag{3}$$

and

$$k_c h = \left[\frac{4(1-\nu_f)(1-\nu_s)}{1-4\nu_s/3}\right]^{1/3} r^{1/3} + d_3 r + d_4 r^{4/3} + d_5 r^{5/3} + \mathcal{O}(r^2), \tag{4}$$

where the coefficients $c_4, \cdots, c_6, d_3, \cdots, d_5$ are shown in Appendix B.

Eq. (2) is used for buckling-based metrology applications to calculate the Young modulus of the film, but is only valid for low strains ($\ll$ 10%) under the assumption of plane strain [15]. However, uni-axial tension does not lead to plane strain and Eq. (3) is more appropriate, and is valid for finite strains. Numerically, we find little difference between the predictions of the two expressions, provided the strains are small. However, as $\nu_f \to \nu_s$, the critical strain becomes large and the linear-elastic results from Eq. (2) greatly underestimate the numerical results from Abaqus and Mathematica, while Eq. (3) gives good agreement, see the example in Fig. 5(a-b) which shows the variations of λ_c and $k_c h$ with ν_f when $\nu_s = 0.495$ (quasi-incompressible substrate)

In Fig. 6(a-b), we plot the variations of λ_c and $k_c h$ with the Poisson ratio of the film ($0 < \nu_f < 0.45$) for different values of shear moduli contrast μ_f/μ_s using Eq. (3)-Eq. (4), because they give curves instantly compared to long computations.

3. Methods

3.1. Semi-analytical treatment

We use Eq. (1) to determine the principal components of the Cauchy stress $\mathbf{T} = J^{-1}\mathbf{F}\left(\partial W/\partial \mathbf{F}\right)$ as

$$T_i = E\frac{J^{-(2\alpha+1)}\left(-\alpha\lambda_i^2 + (\alpha - 1 + \alpha\lambda_i^4)J^{2\alpha} - (\alpha-1)\lambda_i^2 J^{4\alpha}\right)}{2\lambda_i^2\,(1+\nu)}, \tag{5}$$

where the λ_i are the principal stretch ratios and $J = \det \mathbf{F}$.

The substrate is under uniaxial tension along X, so that $T_{22}^s = T_{33}^s = 0$, which gives the following deformation gradient,

$$\mathbf{F}^s = \operatorname{diag}\left(\lambda_1, \lambda_1^{-\nu_s}, \lambda_1^{-\nu_s}\right). \tag{6}$$

The film and substrate are perfectly bonded, so that $\lambda_1^f = \lambda_1^s$, $\lambda_3^f = \lambda_3^s$, and $T_{22}^f = T_{22}^s = 0$. We then find that

$$\mathbf{F}^f = \operatorname{diag}\left(\lambda_1, \lambda_1^{\frac{\nu_f(\nu_s-1)}{(1-\nu_f)}}, \lambda_1^{-\nu_s}\right). \tag{7}$$

To find the critical state of buckling, a small-amplitude mechanical displacement $\mathbf{u}$ is superimposed on the finite deformations. The incremental equations of equilibrium read

$$\mathcal{A}_{0jilm}^s u_{m,lj}^s = 0, \qquad -\infty < y < 0,$$
$$\mathcal{A}_{0jilm}^f u_{m,lj}^f = 0, \qquad 0 < y < h, \tag{8}$$

where the commas denote differentiation with respect to the coordinates, h is the current thickness of the film, and $\mathcal{A}_0$ is the fourth-order tensor of the instantaneous elastic moduli, with components

$$\mathcal{A}_{0jilm} = J^{-1} F_{j\alpha}\frac{\partial^2 W}{\partial F_{i\alpha}\partial F_{m\beta}} F_{l\beta}. \tag{9}$$

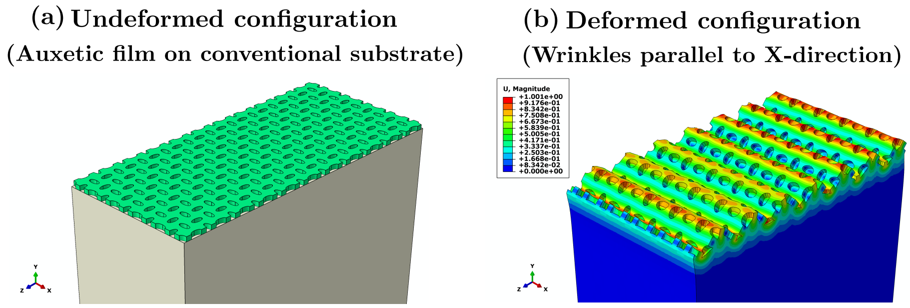

Figure 7: (a) Undeformed and (b) deformed configurations of auxetic stiff film with orthogonal-oval shaped patterns bonded to a compliant substrate. The base materials for film and substrate are incompressible. Periodic boundary conditions are applied on the extreme faces of the domain along X and Z and the system is subjected to uni-axial tension along X. In (b), we observe that the wrinkles are generated parallel to the direction of tension. The critical strain for buckling is $\epsilon_c \simeq 0.274$.

We look for solutions of the forms:

$$u_z = e^{sy}\sin(kz), \qquad u_y = e^{sy}\cos(kz), \tag{10}$$

where s is the attenuation coefficient and k is the wavenumber of the sinusoidal wrinkles. Substitution into Eq. (8) leads to an eigenproblem, with characteristic equation a bicubic in s. In the film, the general solution is of the form

$$u_z^f = \left(\sum_{i=1}^{4} \mathcal{V}_i e^{s_i y}\right)\sin(kz), \quad u_y^f = \left(\sum_{i=1}^{4} \mathcal{V}_i e^{s_i y}\right)\cos(kz), \tag{11}$$

where $s_1, \cdots, s_4$ are the eigenvalues, and $\mathcal{V}_1, \cdots, \mathcal{V}_4$ are constants. In the substrate, the stretch ratios along the Y- and Z-directions are equal, and $s = 1$ is a repeated eigenvalue. The other repeated root, $s = -1$ is discarded to enforce decay. There, the solution is thus of the form

$$u_z^s = (\mathcal{U}_1 + \mathcal{U}_2 y)e^{y}\sin(kz), \qquad u_y^s = (\mathcal{U}_1 + \mathcal{U}_2 y)e^{y}\cos(kz), \tag{12}$$

where $\mathcal{U}_1, \mathcal{U}_2$ are constants.

By applying the traction-free boundary conditions

$$\mathcal{A}^f_{02ilm} u^f_{m,l} = 0, \qquad y = h, \tag{13a}$$

and the continuity conditions

$$\mathcal{A}^f_{02ilm} u^f_{m,l} = \mathcal{A}^s_{02ilm} u^s_{m,l}, \qquad u^f_i = u^s_i, \qquad y = 0, \tag{13b}$$

we obtain six homogeneous equations for $\{\mathcal{U}_1, \mathcal{U}_2, \mathcal{V}_1, \cdots, \mathcal{V}_4\}$. The bifurcation condition is then given by equating the determinant of a 6×6 coefficient matrix to 0.

3.2. Finite Element simulations: 3D models

We first checked the accuracy of our periodic boundary conditions (PBCs) code (Python script) to reproduce known results for wrinkling under plane-strain compression. Hence, we performed a linear buckling analysis in ABAQUS on an incompressible neo-Hookean bilayer periodic along the X-direction, see Appendix A, and recovered the results of [42].

We then perform a series of finite-element simulations for 3D Blatz-Ko model bilayers under uni-axial tension. The dimensions (X, Y, Z) of the bilayer structure are $15 \times 45 \times 5.684$ units with $h_s/h_f = 299$ when the substrate is incompressible, and $15 \times 80 \times 4.504$ units with $h_s/h_f = 399$ when the film is highly auxetic.

The dimensions along the Z-direction are integer multiples of the wavelength (calculated using semi-analytical results from Mathematica) when $(\nu_f, \nu_s) = \{0.3, 0.495\}$ and $\{-0.95, -0.8\}$. For the other (ν_f, ν_s) pairs, we noticed that small variations in the depth of the structure did not notably alter the values of critical stretch (changes in the third decimal point). To save computational time (without compromising the efficiency of the solutions), we kept the dimensions $15 \times 45 \times 5.684$ units and $15 \times 80 \times 4.504$ units when the substrate is incompressible (Section 2.2) and when the film is highly auxetic (Section 2.3).

For the neo-Hookean bilayers ($\alpha_f = \alpha_s = 1$), the dimensions are $6 \times 45 \times 1.85$ units with $h_s/h_f = 299$.

We apply PBCs on the extreme faces in the X- and Z-directions of the domain using a user-defined Python script file. Both the film and substrate are modelled using a UHYPER subroutine with the Blatz-Ko strain energy function. We use a 20-node brick (hexahedral) element with quadratic interpolation and reduced integration (C3D20R) for both film and substrate; for the limiting case of incompressibility, we used a C3D20RH element. For the Blatz-Ko bilayers, 34,200 and 17,130 mesh elements are used for the cases of an incompressible substrate and a highly auxetic film, respectively. For the neo-Hookean bilayer system, 3,240 mesh elements are used.

We find that the numerical results obtained using different approaches in ABAQUS and Mathematica software match well for a wide range of material parameters, see Fig. 4. When $\alpha_f = \alpha_s = 1$ (compressible neo-Hookean bilayers), the results using asymptotic expressions agree well with the numerical simulations, see Fig. 5.

4. Conclusions

We investigated the possibility of harnessing wrinkles parallel to the direction of applied tension in 3D isotropic compressible bilayers subject to large elongations. We paid particular attention to the cases when the substrate is quasi-incompressible and when the film is highly auxetic.

We used a semi-analytical approach with Mathematica to predict the onset of wrinkling, and user-defined Python scripts to apply periodic boundary conditions and UHYPER subroutine for Blatz-Ko material models to perform linear buckling analysis in Finite Element simulations with ABAQUS.

For compressible neo–Hookean bilayer systems, we derived asymptotic expressions for critical stretch ratio and critical wavenumber, which can be used under finite strains to determine the Young modulus of the film layer for buckling-based metrology applications.

We found that wrinkles can be obtained only when the Poisson ratio of the substrate is greater than that of the film. When the Poisson ratios of film and substrate converge to a common value, the critical stretch ratio shoots up sharply and the wavelength of wrinkles is high. In the limit, the wrinkles are not present because there are no compressive stresses developing when the lateral expansions are the same for the film and substrate. Through multiple simulations we showed that by varying the material properties, we can harness or delay the onset of wrinkles.

Some of the limitations of our work include the consideration of isotropic strain energy function for auxetic materials, and deformation-independent material properties. Functional-grading of auxetics could also be explored with the methods presented in this study, see some preliminary works on harnessing instabilities in functionally-graded auxetic materials using tension-field theory [43, 44] and their applications [45–47].

Another area of interest concerns instabilities in materials with auxetic patterns. Indeed, auxetic properties can be obtained at a continuum level with a careful design of holes or voids at the micro-scale [6, 48]. For example, in Fig. 7 we performed linear buckling analysis when the substrate is covered with an initially incompressible film made auxetic by orthogonal oval-shaped voids, leading to an effective Poisson ratio ranging between -0.2 and 0 [9]. We see that the critical stretch ratio $\lambda_c \simeq 1.274$ matches well (within 5%) with the results in Fig. 4.

This paper's analysis could play a critical role in manufacturing and testing the applicability of auxetic hydrogel organ patches [9] and skin grafts [49].

Appendix A: Validation of PBCs code – 2D incompressible neo-Hookean bilayer model

Under uni-axial, plane-strain compression, the theoretical critical strain is $\varepsilon_c = 1/4\left(3\mu_s/\mu_f\right)^{2/3}$ [42].

In Fig. A.1, we applied PBCs on the left and right edges of the domain, roller support on the bottom edge of the substrate, perfect bonding between film and substrate layers, and traction-free condition on the top surface of the film in the two cases $\mu_f/\mu_s = 30, 1000$. We find $\varepsilon_c = 0.053, 0.0052$, respectively, matching well with the theoretical solutions.

Having validated our 1D PBCs script along the X-direction on a 2D model, we then extended the PBCs to two dimensions, along the X- and Z-directions, to perform a linear buckling analysis on 3D bilayer systems under uniaxial tension.

The height ratio of substrate to film layers was taken as $h_s/h_f = 163$, with the width of layers being 30.457 units. We modelled both film and substrate with the incompressible neo-Hookean model.

We used a hybrid 8-node plane strain quadrilateral element with quadratic interpolation and reduced integration (CPE8RH) for both film and substrate layers. We also applied periodic boundary conditions on the left and right edges of the domain. The minimum size of the mesh element is lower than the height of the film. We took 12,800 elements, and the numerical results converged and were consistent with the theoretical solutions.

Appendix B: Coefficients in asymptotic expressions

$$
\begin{aligned}
c_4 &= \frac{\mathcal{C}\left(45 + \nu_s c_{4a} + \nu_f c_{4b} + \nu_f^2 c_{4c}\right)}{20 \times 2^{1/3} \times 3^{2/3}(\nu_f - \nu_s)^2(-1+\nu_s)(-3+4\nu_s)^{4/3}},\\
c_5 &= \frac{\mathcal{C}^2(-1+\nu_f)(-1+2\nu_s)(-3-4\nu_f+4\nu_s)}{2^{2/3} \times 3^{1/3}(\nu_f - \nu_s)^2(-3+4\nu_s)^{5/3}},\\
c_6 &= \frac{4725 - 2\nu_f^4 c_{6a} - \nu_s c_{6b} + \nu_f^3 c_{6c} + \nu_f^2 c_{6d} + 2\nu_f c_{6e}}{12600(3-4\nu_s)^2(-1+\nu_s)^2(-\nu_f+\nu_s)^3},\\
\mathcal{C} &= \left((1-\nu_f)(\nu_s-1)\right)^{1/3},
\end{aligned} \tag{B.1a}
$$

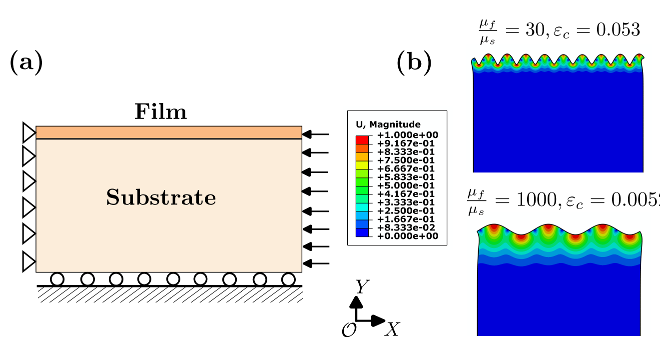

Figure A.1: (a) Schematic representation of an incompressible neo-Hookean stiff film/soft substrate bilayer system under uni-axial compression. On the left edge of the domain, displacement and shear traction are set at zero. On the bottom edge of the domain, roller support restricts vertical displacement and shear traction, and the top surface of the film is traction-free. (b) Linear buckling solutions with critical strains ε_c when $\mu_f/\mu_s = 30, 1000$, in line with the predictions of Cao and Hutchinson [42].

and

$$
\begin{aligned}
c_{4a} &= -64 + (13 - 4\nu_s)\nu_s, \\
c_{4b} &= -71 + \nu_s(66 + (51 - 26\nu_s)\nu_s), \\
c_{4c} &= 56 - 92\nu_s + 26\nu_s^2, \\
c_{6a} &= 33727 + 2\nu_s(-73474 + \nu_s(122601 \\
&\quad + \nu_s(-92584 + 26681\nu_s))), \\
c_{6b} &= 4410 + \nu_s(82574 + \nu_s(-288226 \\
&\quad + \nu_s(399999 - 260716\nu_s + 67034\nu_s^2))), \\
c_{6c} &= 95848 + 2\nu_s(-138872 + \nu_s(46253 \\
&\quad + \nu_s(235988 + \nu_s(-297317 + 106724\nu_s)))), \\
c_{6d} &= -3509 + \nu_s(-202720 + \nu_s(841376 + \nu_s(-1218634 \\
&\quad + \nu_s(643241 + 2(22435 - 53362\nu_s)\nu_s)))), \\
c_{6e} &= -11970 + \nu_s(78479 + \nu_s(-137927 + \nu_s(-12652 \\
&\quad + \nu_s(271583 + \nu_s(-276527 + 89714\nu_s))))).
\end{aligned}
\tag{B.1b}
$$

Similarly, the coefficients of higher-order terms in the asymptotic expression for critical wavenumber (Eq. (4)) are

$$
\begin{aligned}
d_3 &= \frac{4 + 2\nu_s - 11\nu_s^2 + \nu_f\left(11 - 32\nu_s + 26\nu_s^2\right)}{15\left(3 - 7\nu_s + 4\nu_s^2\right)}, \\
d_4 &= \frac{\left(\frac{2}{3}\right)^{2/3}\mathcal{C}(1 + 2\nu_f)(-1 + 2\nu_s)}{(-3 + 4\nu_s)^{4/3}}, \\
d_5 &= \frac{\mathcal{C}^2\left(-6761 + \nu_s d_{5a} + 4\nu_f^2 d_{5b} - 2\nu_f d_{5c}\right)}{3150 \times 2^{2/3} \times 3^{1/3}(-1 + \nu_f)(-1 + \nu_s)^3(-3 + 4\nu_s)^{5/3}},
\end{aligned}
\tag{B.2a}
$$

and

$$
\begin{aligned}
d_{5a} &= 21724 + \nu_s(-19146 + \nu_s(-2636 + 7519\nu_s)), \\
d_{5b} &= 646 + \nu_s(-4964 + \nu_s(12906 \\
&\quad + \nu_s(-14204 + 5791\nu_s))), \\
d_{5c} &= -3821 + \nu_s(7864 + \nu_s(5844 \\
&\quad + \nu_s(-22796 + 13609\nu_s))).
\end{aligned}
\tag{B.2b}
$$

CRediT authorship contribution statement

Sairam Pamulaparthi Venkata: Original writing and numerical simulations. **Yuxin Fu:** Numerical simulations and writing. **Yibin Fu:** Mathematica code and writing. **Valentina Balbi:** Editing and writing. **Michel Destrade:** Conceptualisation, editing and writing.

Declaration of Competing Interest

The authors declare that they have no known competing financial interests or personal relationships that could have appeared to influence the work reported in this paper.

Acknowledgments

This project has received funding from the European Union's Horizon 2020 research and innovation programme under the Marie Skłodowska-Curie Grant Agreement No. 956401.

Supplementary data

There is no Supplementary material attached to this article.

References

[1] S. Timoshenko, History of Strength of Materials: With a Brief Account of the History of Theory of Elasticity and Theory of Structures, Dover Publications, New York, 1983.

[2] S. Mueller, B. Kruck, P. Baudisch, Laserorigami: Laser-cutting 3d objects, in: Proceedings of the SIGCHI Conference on Human Factors in Computing Systems, CHI '13, Association for Computing Machinery, New York, NY, USA, 2013, p. 2585–2592. DOI:10.1145/2470654.2481358.

[3] S. Sun, M. Brandt, M. Easton, Powder bed fusion processes: An overview, Laser Additive Manufacturing (2017) 55–77. DOI:10.1016/B978-0-08-100433-3.00002-6.

[4] M. Y. Popereka, V. Balagurov, Ferromagnetic films having a negative Poisson ratio, Soviet Physics, Solid state 11 (1970) 2938–2943.

[5] F. Milstein, K. Huang, Existence of a negative Poisson ratio in fcc crystals, Physical Review B 19 (1979) 2030. DOI:10.1103/PhysRevB.19.2030.

[6] R. Lakes, Advances in negative Poisson's ratio materials, 1993. DOI:10.1002/adma.19930050416.

[7] W. J. S. Dolla, B. A. Fricke, B. R. Becker, Structural and Drug Diffusion Models of Conventional and Auxetic Drug-Eluting Stents, Journal of Medical Devices 1 (2006) 47–55. DOI:10.1115/1.2355691.

[8] A. Lazarus, P. M. Reis, Soft actuation of structured cylinders through auxetic behavior, Advanced Engineering Materials 17 (2015) 815–820. DOI:10.1002/adem.201400433.

[9] P. Chansoria, J. Blackwell, E. L. Etter, E. E. Bonacquisti, N. Jasiewicz, T. Neal, S. A. Kamal, J. Hoque, S. Varghese, T. Egan, J. Nguyen, Rationally designed anisotropic and auxetic hydrogel patches for adaptation to dynamic organs, Advanced Functional Materials 32 (2022) 2207590. DOI:10.1002/adfm.202207590.

[10] N. Bowden, S. Brittain, A. G. Evans, J. W. Hutchinson, G. M. Whitesides, Spontaneous formation of ordered structures in thin films of metals supported on an elastomeric polymer, Nature 393 (1998) 146–149. DOI:10.1038/30193.

[11] S. Wagner, S. P. Lacour, J. Jones, P. hui I. Hsu, J. C. Sturm, T. Li, Z. Suo, Electronic skin: architecture and components, Physica E: Low-dimensional Systems and Nanostructures 25 (2004) 326–334. Proceedings of the 13th International Winterschool on New Developments in Solid State Physics - Low-Dimensional Systems. DOI:10.1016/j.physe.2004.06.032.

[12] D.-Y. Khang, H. Jiang, Y. Huang, J. A. Rogers, A stretchable form of single-crystal silicon for high-performance electronics on rubber substrates, Science 311 (2006) 208–212. DOI:10.1126/science.1121401.

[13] J. Zhang, Y. Li, Y. Xing, Theoretical and experimental investigations of transient thermo-mechanical analysis on flexible electronic devices, International Journal of Mechanical Sciences 160 (2019) 192–199. DOI:10.1016/j.ijmecsci.2019.04.041.

[14] C. Harrison, C. M. Stafford, W. Zhang, A. Karim, Sinusoidal phase grating created by a tunably buckled surface, Applied Physics Letters 85 (2004) 4016–4018. DOI:10.1063/1.1809281.

[15] C. M. Stafford, C. Harrison, K. L. Beers, A. Karim, E. J. Amis, M. R. VanLandingham, H.-C. Kim, W. Volksen, R. D. Miller, E. E. Simonyi, A buckling-based metrology for measuring the elastic

moduli of polymeric thin films, Nature Materials 3 (2004) 545–550. DOI:10.1038/nmat1175.

[16] J. Huang, M. Juszkiewicz, W. H. de Jeu, E. Cerda, T. Emrick, N. Menon, T. P. Russell, Capillary wrinkling of floating thin polymer films, Science 317 (2007) 650–653. DOI:10.1126/science.1144616.

[17] P.-C. Lin, S. Yang, Mechanically switchable wetting on wrinkled elastomers with dual-scale roughness, Soft Matter 5 (2009) 1011–1018. DOI:10.1039/B814145B.

[18] A. J. Crosby, Why should we care about buckling?, Soft Matter 6 (2010) 5660–5660. DOI:10.1039/C0SM90040K.

[19] Z. Cai, Y. Fu, On the imperfection sensitivity of a coated elastic half-space, Proceedings of the Royal Society of London. Series A: Mathematical, Physical and Engineering Sciences 455 (1999) 3285–3309. DOI:10.1098/rspa.1999.0451.

[20] K. Efimenko, M. Rackaitis, E. Manias, A. Vaziri, L. Mahadevan, J. Genzer, Nested self-similar wrinkling patterns in skins, Nature Materials 4 (2005) 293–297. DOI:10.1038/nmat1342.

[21] A. Goriely, M. Ben Amar, Differential growth and instability in elastic shells, Phys. Rev. Lett. 94 (2005) 198103. DOI:10.1103/PhysRevLett.94.198103.

[22] C. M. Stafford, S. Guo, C. Harrison, M. Y. M. Chiang, Combinatorial and high-throughput measurements of the modulus of thin polymer films, Review of Scientific Instruments 76 (2005) 062207. DOI:10.1063/1.1906085.

[23] H. Li, S. Cai, Y. Zhang, K.-C. Hwang, Y. Ma, X. Feng, Local wrinkling versus global buckling of stiff film bonded to finite-thick substrate, Extreme Mechanics Letters 29 (2019) 100453. DOI:https://doi.org/10.1016/j.eml.2019.100453.

[24] Y. Cao, J. W. Hutchinson, From wrinkles to creases in elastomers: the instability and imperfection-sensitivity of wrinkling, Proceedings of the Royal Society A: Mathematical, Physical and Engineering Sciences 468 (2012) 94–115. DOI:10.1098/rspa.2011.0384.

[25] F. Brau, P. Damman, H. Diamant, T. A. Witten, Wrinkle to fold transition: influence of the substrate response, Soft Matter 9 (2013) 8177–8186. DOI:10.1039/C3SM50655J.

[26] L. Zhuo, Y. Zhang, From period-doubling to folding in stiff film/soft substrate system: The role of substrate nonlinearity, International Journal of Non-Linear Mechanics 76 (2015) 1–7. DOI:https://doi.org/10.1016/j.ijnonlinmec.2015.05.002.

[27] D. Bigoni, N. Bordignon, A. Piccolroaz, S. Stupkiewicz, Bifurcation of elastic solids with sliding interfaces, Proceedings of the Royal Society A: Mathematical, Physical and Engineering Sciences 474 (2018) 20170681. DOI:10.1098/rspa.2017.0681.

[28] A. D. Bakiler, A. Javili, Understanding the role of interfacial mechanics on the wrinkling behavior of compressible bilayer structures under large plane deformations, Mathematics and Mechanics of Solids 28 (2023) 748–772. DOI:10.1177/10812865221094833.

[29] S. Nikravesh, D. Ryu, Y.-L. Shen, Surface instability of composite thin films on compliant substrates: Direct simulation approach, Frontiers in Materials 6 (2019). DOI:10.3389/fmats.2019.00214.

[30] A. L. Volynskii, S. Bazhenov, O. V. Lebedeva, N. F. Bakeev, Mechanical buckling instability of thin coatings deposited on soft polymer substrates, Journal of Materials Science 35 (2000) 547–554. DOI:10.1023/A:1004707906821.

[31] ABAQUS Inc., ABAQUS/Standard User's Manual, Version 2019, Dassault Systèmes Simulia Corp, United States, 2019.

[32] Wolfram Research Inc., Mathematica, Version 13.1, Champaign, IL, 2022. URL: https://www.wolfram.com/mathematica.

[33] A. Bonfanti, A. Bhaskar, Elastic stabilization of wrinkles in thin films by auxetic microstructure, Extreme Mechanics Letters 33 (2019) 100556. DOI:10.1016/j.eml.2019.100556.

[34] P. J. Blatz, W. L. Ko, Application of finite elastic theory to the deformation of rubbery materials, Transactions of the Society of Rheology 6 (1962) 223–252. DOI:10.1122/1.548937.

[35] J. Crespo, F. J. Montáns, A continuum approach for the large strain finite element analysis of auxetic materials, International Journal of Mechanical Sciences 135 (2018) 441–457. DOI:10.1016/j.ijmecsci.2017.11.038.

[36] J. Ciambella, G. Saccomandi, A continuum hyperelastic model for auxetic materials, Proceedings of the Royal Society A: Mathematical, Physical and Engineering Sciences 470 (2014) 20130691.

[37] J. B. Choi, R. S. Lakes, Non-linear properties of metallic cellular materials with a negative poisson's ratio, Journal of Materials Science 27 (1992) 5375–5381. DOI:10.1007/BF02403846.

[38] S. Nikravesh, D. Ryu, Y.-L. Shen, Direct numerical simulation of buckling instability of thin films on a compliant substrate, Advances in Mechanical Engineering 11 (2019) 1687814019840470. DOI:10.1177/1687814019840470.

[39] J. Y. Chung, A. J. Nolte, C. M. Stafford, Surface wrinkling: A versatile platform for measuring thin-film properties, Advanced Materials 23 (2011) 349–368. DOI:10.1002/adma.201001759.

[40] Z. Cai, Y. Fu, Exact and asymptotic stability analyses of a coated elastic half-space, International Journal of Solids and Structures 37 (2000) 3101–3119. DOI:10.1016/S0020-7683(99)00071-2.

[41] Z. Cai, Y. Fu, Effects of pre-stretch, compressibility and material constitution on the period-doubling secondary bifurcation of a film/substrate bilayer, International Journal of Non-Linear Mechanics 115 (2019) 11–19. DOI:https://doi.org/10.1016/j.ijnonlinmec.2019.05.001.

[42] Y. Cao, J. W. Hutchinson, Wrinkling Phenomena in Neo-Hookean Film/Substrate Bilayers, Journal of Applied Mechanics 79 (2012) 031019. DOI:10.1115/1.4005960.

[43] S. P. Venkata, V. Balbi, M. Destrade, D. Accoto, G. Zurlo, Programmable wrinkling for functionally-graded auxetic circular membranes, Extreme Mechanics Letters 63 (2023) 102045. DOI:10.1016/j.eml.2023.102045.

[44] S. Pamulaparthi Venkata, V. Balbi, M. Destrade, G. Zurlo, Designing necks and wrinkles in inflated auxetic membranes, International Journal of Mechanical Sciences 268 (2024) 109031. DOI:10.1016/j.ijmecsci.2024.109031.

[45] Q. Zhao, J. Wang, H. Cui, H. Chen, Y. Wang, X. Du, Programmed shape-morphing scaffolds enabling facile 3d endothelialization, Advanced Functional Materials 28 (2018) 1801027.

[46] Y. Zahoor, R. De Breuker, M. Voskuijl, Preliminary design of a te morphing surface for rotorcraft, in: AIAA Scitech 2020 Forum, 2020, p. 1301.

[47] J. Babič, M. Laffranchi, F. Tessari, T. Verstraten, D. Novak, N. Šarabon, B. Ugurlu, L. Peternel, D. Torricelli, J. F. Veneman, Challenges and solutions for application and wider adoption of wearable robots, Wearable Technologies 2 (2021) e14.

[48] K. Bertoldi, V. Vitelli, J. Christensen, M. Van Hecke, Flexible mechanical metamaterials, Nature Reviews Materials 2 (2017) 1–11. DOI:10.1038/natrevmats.2017.66.

[49] V. Gupta, A. Chanda, Biomechanical Modelling of Hierarchical Metamaterials for Skin Grafting, Springer Nature Singapore, Singapore, 2023, pp. 71–83. DOI:10.1007/978-981-99-5064-5_4.